Sensors & Actuators: B. Chemical 346 (2021) 130510

Contents lists available at ScienceDirect

Sensors and Actuators: B. Chemical

journal homepage: www.elsevier.com/locate/snb

An efficient hydrogen gas sensor based on hierarchical Ag/ZnO hollow microstructures

Sonalika Agarwal [a,*], Sanjay Kumar [a], Himanshu Agrawal [a], Mohamad G. Moinuddin [b], Manoj Kumar [a], Satinder K. Sharma [b], Kamlendra Awasthi [a,c,*]

[a] Department of Physics, Malaviya National Institute of Technology, Jaipur, Rajasthan, 302017, India
[b] School of Computing and Electrical Engineering (SCEE), Indian Institute of Technology (IIT)-Mandi, 175005, Himachal Pradesh, India
[c] Materials Research Centre, Malaviya National Institute of Technology, Jaipur, Rajasthan, 302017, India

ARTICLE INFO

Keywords:
Hydrogen sensors
Silver
Zinc oxide
Hollow microstructures

ABSTRACT

The design of hierarchical zinc oxide (ZnO) microstructures modified with silver (Ag) nanoparticles have emerged as an effective approach for improving the hydrogen gas sensing performance. Here, we report a simple, low-cost chemical co-precipitation method to obtain the Ag/ZnO hollow microstructures and morphologically characterized them by field emission scanning electron microscopy (FESEM). FESEM images revealed the clear hollow hexagonal tube-like morphology. The existence of Ag in ZnO was confirmed by X-ray diffraction (XRD) and energy-dispersive X-ray spectroscopy (EDS). UV visible absorption and photoluminescence (PL) spectra were also recorded to observe the effect of Ag nanofiller on the optical properties of ZnO. Furthermore, the gas sensing properties of the as-prepared bare ZnO and Ag/ZnO sensor were investigated. The thoroughly sensing experiments demonstrated that after modification with Ag nanoparticles the ZnO sensor shows superior sensitivity 479 % towards 300 ppm hydrogen gas concentration, whereas 101 % response was noted for the pure ZnO sensor at 250 °C working temperature. Meanwhile, Ag/ZnO hybrids exhibited excellent selectivity, fast response, and recovery time and also obtained a good and stable response signal at 5 ppm H_2 exposure, which indicated that the lower concentration measurement is also attainable. This enhancement in the sensing performance of Ag/ZnO structures towards hydrogen is due to the chemical and electronic sensitization effect of Ag nanoparticles. As a result, such microstructure is attributed to more oxygen species and active sites, and it enhances the sensitivity of a sensor. Moreover, this type of hybrid opens a new path and supports the next generation of innovative materials to fabricate highly selective and sensitive H_2 gas sensing devices.

1. Introduction

To achieve the goal of reduction of greenhouse gases and global warming, alternative renewable energy sources are imperative to replace fossil fuels. In this respect, hydrogen gas (H_2) is considered a potential alternative as a green, renewable, and abundant fuel in the future for several applications, including fuel cells, automobiles, power generators, aircraft, and space missions [1,2]. However, H_2 is odorless, light, tasteless, colorless, flammable, and exceedingly explosive in the concentration range of 4–75 vol%. It may result in disastrous consequences, such as an accidental explosion in case of leakages during the production, storage, and transportation of hydrogen gas. Therefore a highly sensitive material will be an indispensable part of fabricating a low-cost H_2 sensor with high sensitivity, fast response, short recovery time, long-term stability, and good repeatability [3]. To overcome, these problems associated with the stated systems, now the researchers aim to develop highly sensitive and precise sensors based on chemi-resistive sensors due to their various features such as low cost, online response, high sensitivity, portability, and easy fabrication and operation [4,5]. The chemi-resistive sensors work on the principle of measuring the change in the resistance of the sensitive layer when it interacts with the target gas.

Among them, ZnO is an n-type metal oxide with a wide bandgap of ~3.37 eV [6,7] and is widely used for hydrogen sensing applications due to its high sensitivity, low cost, fast response time, simply controlled electronics, and long-term stability to other semiconductors [8–10] but it suffers from high operating temperature and low selectivity [11]. In this context, doping, surface modification, and functionalization with

* Corresponding authors at: Department of Physics, Malaviya National Institute of Technology, Jaipur, Rajasthan, 302017, India.
E-mail addresses: sonalika.spsl@gmail.com (S. Agarwal), kawasthi.phy@mnit.ac.in (K. Awasthi).

https://doi.org/10.1016/j.snb.2021.130510
Received 25 May 2021; Received in revised form 26 July 2021; Accepted 26 July 2021
Available online 29 July 2021

different noble metals nanoparticles such as Pt, Pd, Ag, and Au are highly recommended ways to improve the selectivity and response of the ZnO sensor [12–15].

In particular, the modification/doping with Ag nanoparticles has been widely used because of their low cost and excellent catalytic properties [16,17]. Ag nanoparticles act as catalysts to accelerate the chemisorption process of ambient oxygen. The target gas molecules on metal oxide's surface generate additional adsorption sites, which greatly improve their gas-sensing performance [18]. Moreover, silver is one of the best alternative metals because of its high solubility, larger ionic size, and minimum orbital energy. Many Ag/ZnO-based gas sensors have been reported for detecting different gases such as ethanol, H_2S, ammonia, acetone, CO, NO_2, C_2H_2, etc [19–21]. Wang et al. [22] modified the ZnO nanoparticles with Ag nanoparticles of different wt% (0, 1, 3 & 5%). The 3 wt% Ag-ZnO sensors achieved the highest value of response of 298 at 10 ppm H_2S exposure and also showed the fast response (5 s) and recovery times (9 s), respectively for ethanol gas. Zhang et al. [23] prepared Ag-ZnO nanoparticles, which showed superior sensing properties to NO_2 at room temperature under visible light irradiation. Ding et al. [24] reported the ZnO-Ag hybrids, which exhibited superior sensing properties and response value (101.8) towards 100 ppm of ethanol, which is much higher than the response of pure ZnO. Dilova et al. [25] fabricated Ag-doped ZnO 3D nanostructures and observed the effect of light irradiation on gas sensing properties and achieved a strong and stable response ($\Delta R/R_0 \sim 13$; where R_0 and ΔR are steady-state resistance and resistance change due to chemi-adsorption, respectively) at 1 ppm CO exposure. Zhou et al. [26] reported the synthesis, characterization and C_2H_2 sensing properties of Ag modified ZnO nanorods, which showed a superior response 539 for 100 ppm C_2H_2. Tsai et al. [27] developed the NO sensor based on Ag-doped ZnO nanoflowers and UV-LED illumination was applied for improving the sensing properties for the NO sensor from 73.91 to 89.04 %.

According to the above-reported studies and the best of our knowledge, H_2 sensing performances of Ag/ZnO hybrids have not been reported yet. Hence, the study of hydrogen gas detection based on Ag/ZnO microstructures is the prime motive of our research, which is presented in the current work. Therefore, we are reporting first time the effect of Ag nanoparticles (NPs) on the ZnO to enhance the sensing properties for hydrogen gas. In this study, ZnO hollow hexagonal-shaped tube-like microstructures modified with Ag nanoparticles were developed as a new hydrogen sensing material by using a one-step simple chemical co-precipitation method without using any surfactant and reducing agents. To demonstrate this new concept, the bare ZnO and Ag/ZnO sensors were tested for the detection of H_2, CO, and CO_2 gases over a wide range of operating temperatures. The results showed that incorporation of Ag nanoparticles in ZnO can greatly enhance the gas sensing properties and exhibits the highest response of 479 % to hydrogen gas at 300 ppm concentration. Furthermore, both sensors showed higher selectivity towards H_2 gas and the detection limit of the Ag/ZnO sensor was 5 ppm for hydrogen gas. Finally, a possible gas sensing mechanism is proposed and explained in detail.

2. Experimental section

2.1. Synthesis of ZnO and Ag/ZnO hollow microstructures

All of the chemicals were of analytical grade and used without further purification. The chemical co-precipitation method was adopted for the synthesis of Ag/ZnO hollow hexagonal-shaped microstructures. In this experiment, solution-A was prepared by dissolving 1 wt% silver nitrate ($AgNO_3$) and 2.97 g Zinc nitrate hexahydrate ($Zn(NO_3)_2{\cdot}6H_2O$), in 100 mL of Distilled (DI) water, and solution-B was prepared by dissolving 1.40 g hexamethylenetetramine (HMT) in again 100 mL of DI water. We mixed solution-B with solution-A, dropwise under mild magnetic stirring for 1 h to become a homogenous solution. Then the resultant homogenous solution was stored at 100 °C for 36 h. Subsequently, this product was collected by centrifugation, washed several times to remove the impurities with distilled water, and finally dried at 60 °C. As a resultant, obtained powder was calcined at 500 °C for 2 h. Earlier we used the same method to prepare the ZnO microstructures (without using the $AgNO_3$).

2.2. Characterization

Then we examined experimentally developed materials crystal structures by using powder X-ray diffraction (XRD, Panalytical XPert Pro X-ray diffractometer) with Cu-Kα ($\lambda = 1.5406$ Å) radiation source and 2θ range was 20° to 80°. Field emission scanning electron microscopy (FESEM, Nova Nano FE-SEM 450 FEI) was used to observe the prepared samples' morphology and size. The elemental composition was determined by using energy-dispersive X-ray spectroscopy (EDS) attached with FESEM. For investigation & evaluation of the bandgap of microstructures, UV–vis absorption spectrums with the range of wavelength from 200–800 nm by UV–vis NIR spectrophotometer (UV–vis, LAMBDA 750 Perkin Elmer). The photoluminescence (PL) measurements were recorded at room temperature using LABHR-UV-EVO and a He-Cd laser (325 nm) with 30 mW of power.

2.3. Sensor fabrication and gas sensing measurement

Micro interdigital electrodes (μ-IDE) for MOF-based sensors were fabricated using standard semiconductor processing. Initially, the Si (100) wafer was RCA [28] cleaned and thermally oxidized to minimize the leakage current. The ~289 nm thick SiO_2 were grown using CMOS thermal oxidation of Si (100) at 1050 °C for 4 h. The oxidized wafer was diced and undergone micro-lithography and Pt/Cr metallization process as reported earlier [29]. The leakage current between two electrodes was minimal in the range of ~12 pA (~83 GΩ) due to the insulating SiO_2 layer. The fabricated μ-IDE showed an active area of 1×0.5 mm^2 with a uniform finger width/spacing of 50 μm. Furthermore, 5 mg of the as-obtained ZnO and Ag/ZnO powders were ground using a mortar pestle to make a fine paste in ethylene glycol. Then, the connection area on IDEs was covered with tape as shown in Fig. 1. After that, the IDEs were coated with the material paste using the doctor blade method and dried at 60 °C for 12 h. The tape was removed and the sensors were heated at 500 °C for 2 h in the presence of air for better adhesion of the material on the IDEs.

Gas sensing measurements were performed at atmospheric pressure utilizing a stainless-steel chamber with a volume of 250 ml (Fig. 2). The chamber was equipped with a sample stage containing a resistive heater which was controlled by a computer synchronized power supply. The sample stage's temperature was measured and fed back to the loop to control the temperature with a precision of 0.5 °C. The chamber was connected to two mass flow controllers: one for target gas and another for carrier gas i.e. dry air (20 % O_2/ 80 % N_2). The target concentration was achieved by adjusting the flow rates of the mass flow controllers. The total flow rate was kept at 200 sccm throughout the experiment. The resistance of the sensor was measured by the Keithley-2601B electrometer unit by sourcing the voltage (bias voltage: 1 V) and measuring the current. The whole system was controlled by a computer system and integrated by a LabView-based program. The sensor response was calculated by the eqn. (1):

$$S\% = \frac{(R_a - R_g)}{R_g} \times 100 \quad (1)$$

where S is the sensor response, R_a is the resistance in the air and R_g is the resistance in presence of target gas [30,31].

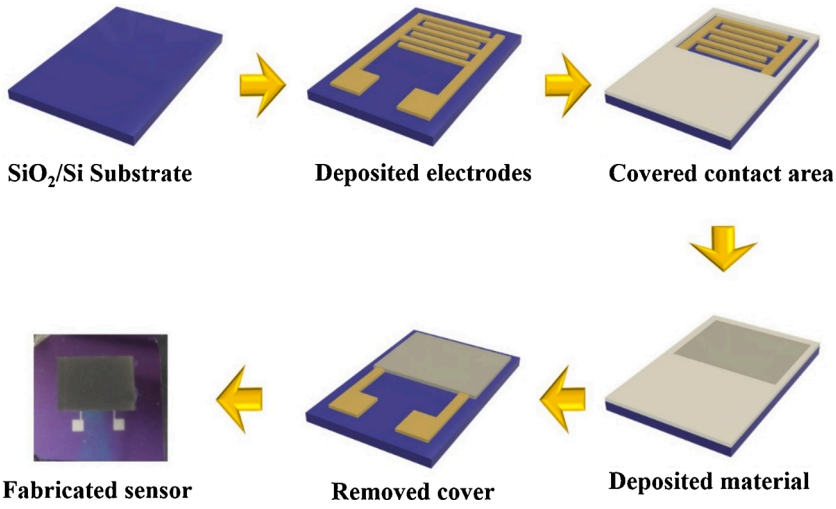

Fig. 1. Schematic for the sensor fabrication.

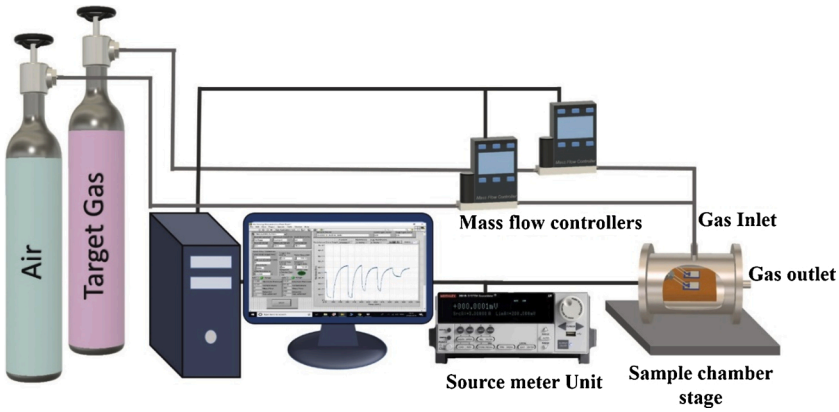

Fig. 2. Schematic of the gas sensing setup.

3. Results and discussion

3.1. Structural properties

Following the successful synthesis of the pristine ZnO and Ag/ZnO hollow microstructures, their crystallographic information was examined using XRD. Fig. 3 shows the diffraction patterns of ZnO and Ag-loaded ZnO nanotubes. In both XRD patterns, peaks centered at 2θ = 31.77, 34.44, 36.26, 47.54, 56.59, 62.86, 66.38, 67.95, 69.09, 72.56, 76.97 degrees are identical to ZnO planes of (100), (002), (101), (102), (110), (103), (200), (112), (201), (004) and (202), respectively and these were gladly indexed to the wurtzite structure (hexagonal phase, space group P 63 mc and lattice parameters a = b = 3.2498 A° and c = 5.2069 A°), which is consistent with the standard card (JCPDS No: 01-076-0704). In the case of the Ag/ZnO sample, there are three others diffraction peaks observed and located at 38.14°, 44.32°, and 64.47°, which are attributed to (111), (200), and (220) planes of face-centered cubic (fcc) lattice for Ag (JCPDS No: 00-004-0783), indicative of the presence of Ag in obtained hybrids microstructures. The phase percent of Ag is 3% and ZnO is 97 % was observed from the quantization chart, shown in the inset of Fig. 3. Furthermore, no characteristic peaks of additional impurities are identified, suggesting the high purity of the samples.

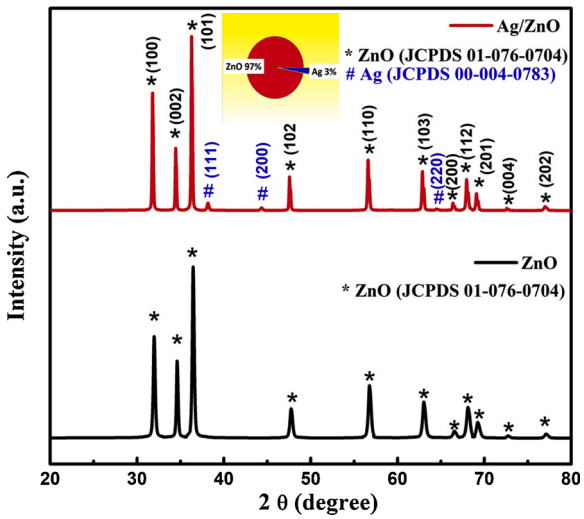

Fig. 3. XRD patterns of the ZnO and Ag/ZnO microstructures; in inset quantification chart of Ag/ZnO microstructure.

3.2. Surface morphology and elemental studies

The information regarding the morphology of bare ZnO and Ag/ZnO composite is attained by FESEM analysis. Fig. 4a shows the FESEM image of as-synthesized ZnO without Ag annealed at 500 °C and confirms the tubes-like microstructures of ZnO having a width in the range 2–3 μm and the average length is 9 μm. Also, at some places, some small

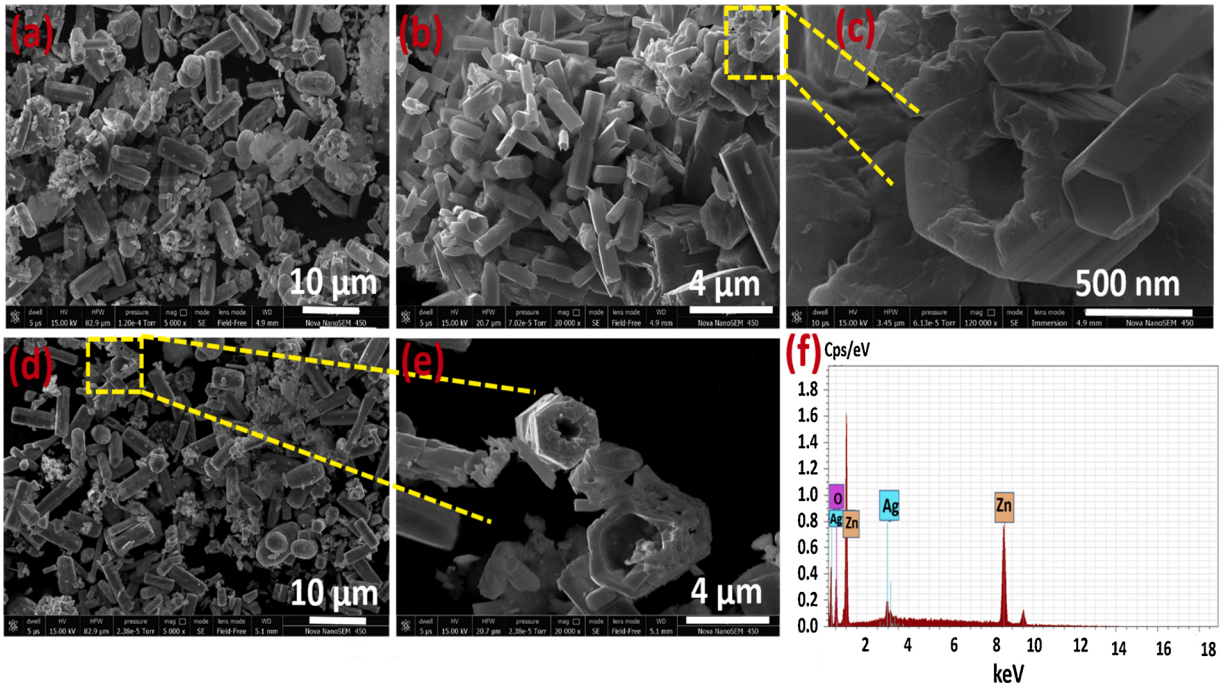

Fig. 4. (a) & (b) low magnification FESEM images of ZnO microstructures (c) high magnification FESEM image of ZnO microstructures (d) low magnification FESEM image of Ag/ZnO microstructures (e) high magnification FESEM image of Ag/ZnO microstructures (f) EDS spectrum of Ag/ZnO microstructures.

tubes can be easily seen in Fig. 4a and seem to be agglomerated. The FESEM image of small tubes with 2–3 µm length is displayed in Fig. 4b. The magnified image (Fig. 4c) of the yellow box indicates that these tubes have a hollow hexagonal cross-section with a diameter of about 500 nm to 1 µm. Fig. 4d shows the FESEM image of ZnO with Ag annealed at 500 °C. Like the ZnO, Ag/ZnO also has the same tube-like morphology and small tubes at some places. The clear hollow hexagonal structure was observed and marked with a yellow area displayed in Fig. 4e. These hollow microstructures play an important role in gas sensing. Due to the resolution limit of the FESEM technique and the small sizes of Ag nanoparticles, it's not easy to find Ag nanoparticles on the surface of ZnO tubes from SEM images. Therefore, to demonstrate the presence of Ag nanoparticles, the Ag/ZnO composite is further characterized by EDS, shown in Fig. 4f. The EDS results specify that Ag/ZnO is made up of only three elements Ag, Zn, and O and their weight/atomic percentage is shown in Table 1. The weight ratios of Zn, O, and Ag are 87.36 %, 5.14 %, and 7.50 %, and the atomic ratios of Zn, O, and Ag are 77.37 %, 18.60 %, and 4.03 %, respectively. It confirms Ag in ZnO, which approves the purity of the sample and is consistent with the XRD results (Fig. 3).

3.3. Growth mechanism of ZnO nanotubes

The growth mechanism consists (Fig. 5) of two subsequent stages in the formation of nanotube structures. Initially, the growth of hexagonal nanorods takes place in the 0001 direction preferentially at the temperature of 100 °C. It is due to the presence of HMT in the precursor solution, which suppresses the growth in the lateral direction. Since these nanorod-like structures possess both polar faces (0001 and $000\bar{1}$) as well as non-polar lateral faces ($00\bar{1}0$ and 1120) [32]. Among which the meta-stable polar faces have lower stability with respect to the lateral faces. The second stage occurs when the temperature of the reaction comes down, then the dissolution of ZnO occurs at the polar faces, thus creating the hollow structures referred to as nanotubes [33].

Table 1
The weight/atomic percent of Zn, O and Ag elements in Ag/ZnO microstructures from EDS spectra.

Element-series	Weight %	Atomic %
Zn-K	87.36	77.37
O-K	5.14	18.60
Ag-L	7.50	4.03
Total	100	100

3.4. UV–vis and photoluminescence analysis

To study the optical properties, UV–vis. spectrums of ZnO and Ag/ZnO microstructures were recorded from the range 300–800 nm and shown in Fig. 6a. A single and strong absorption peak in the UV region at 370 nm of pure ZnO is clearly observed, which is attributed to the wurtzite hexagonal structure of ZnO, and for Ag/ZnO, it is observed at 377 nm. Furthermore, the addition of Ag nanoparticles to the ZnO moved the absorption peak towards a higher wavelength representing the redshift. This redshift is occurred due to the strong interfacial coupling between Ag and ZnO and indicates the changes in bandgap energy of the materials [34,35]. The bandgap energy of the microstructures was attained from plotting the curve of $(\alpha h\nu)^2$ as a function of photon energy ($h\nu$), according to the well-known Tauc's relation: $(\alpha h\nu)^2 = A\,(h\nu - Eg)$ and displayed in the inset of Fig. 6a. The obtained values of bandgap energy were 3.14 and 3.06 eV for ZnO and Ag/ZnO microstructures, respectively. This reduction in the energy band gap on Ag/ZnO materials proposes a better distribution of Ag nanoparticles on the surface of ZnO and led to an increase in the whole absorption visible spectrum range. Therefore, the efficiency of Ag incorporated ZnO materials increases and is good for their use in sensing and optoelectronic devices [36]. More information about the optical properties can be obtained from photoluminescence (PL) spectra.

The room temperature PL spectra with an excitation wavelength of 325 nm of ZnO and Ag/ZnO are shown in Fig. 6b. It can be revealed that both samples show similar emission bands. One is in the UV range, which is narrow excitonic near-band-edge (NBE) emission and is usually ascribed to the free exciton recombination [8,37]. A redshift (382 nm–388 nm was observed in the UV band with Ag doping in ZnO. Second is in the visible range from 450 to 750 nm, known as broader

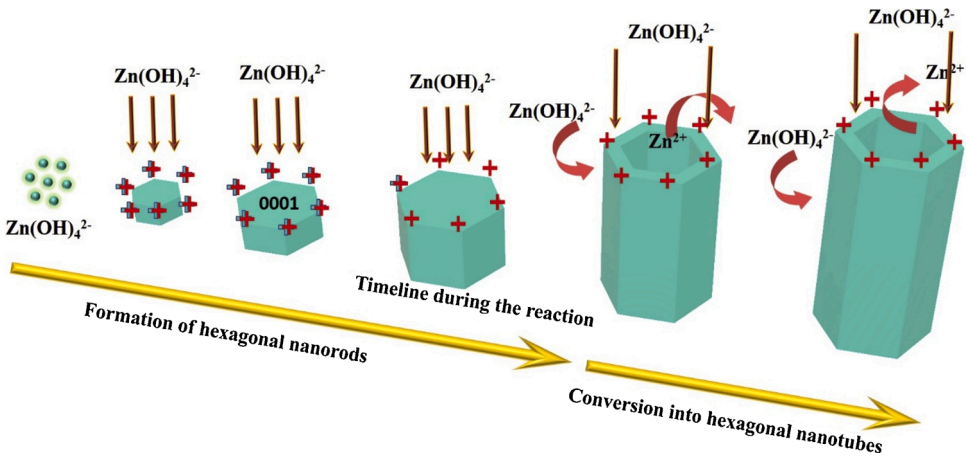

Fig. 5. Schematic illustration of growth mechanism for the formation of nanotubes-like structures of ZnO.

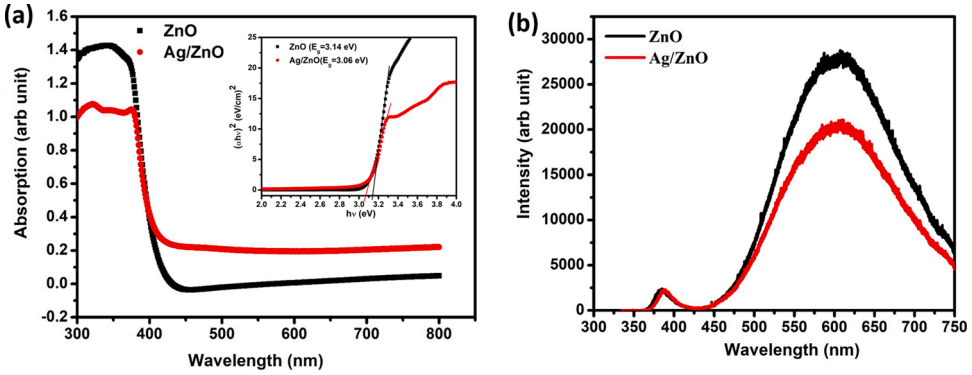

Fig. 6. (a) UV–vis absorption spectra of ZnO and Ag/ZnO microstructures (in the inset: tauc plot between $(\alpha h\nu)^2$ vs $h\nu$ for calculating energy bandgap) and (b) room temperature PL spectra of ZnO and Ag/ZnO microstructures.

deep-level emission (DLE) band and usually due to the charge carrier relaxation via surface-related trap states, intrinsic defects, and extrinsic defects e.g. oxygen vacancies, zinc interstitials, etc., which are advantageous for the performance of a gas sensor, as defects are favorable sites for adsorption of target gases [38]. Furthermore, it is also observed that Ag nanoparticles' incorporation can decrease the PL intensity. This decrease in PL intensity with Ag loading could be associated with the fact that Ag nanoparticles can effectively block the recombination of electron–hole pairs, which is better for adsorption of oxygen molecules on the surface of ZnO in gas sensing detection [22].

3.5. Gas sensing properties

The sensitivity of fabricated ZnO and Ag/ZnO sensing devices was investigated. It is well known that the working temperature plays an important role in the gas sensing properties. Thus, the temperature-

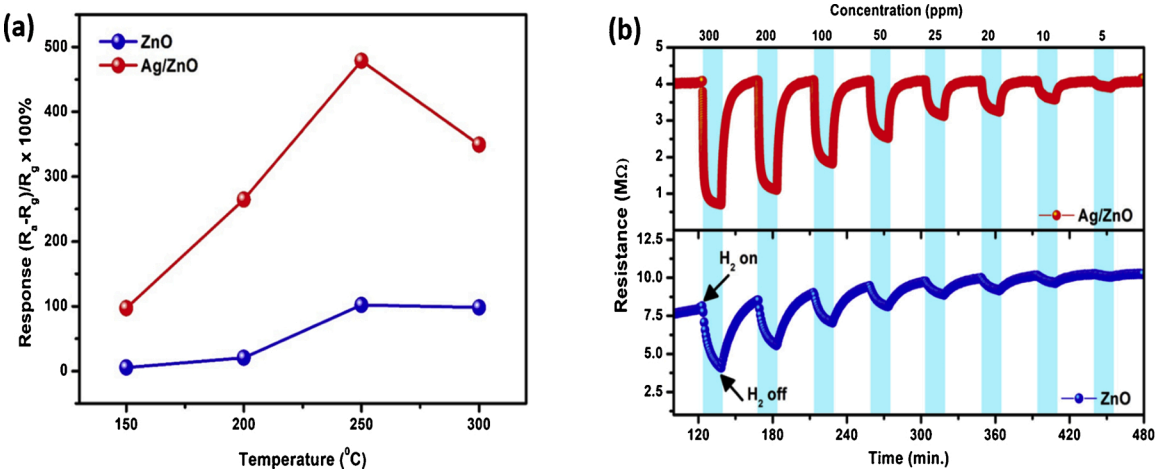

Fig. 7. (a) Temperature-dependent gas sensing response of ZnO and Ag/ZnO sensors towards 300 ppm hydrogen (b) dynamic response/recovery curves of ZnO and Ag/ZnO sensors at different concentrations of hydrogen at optimum temperature 250 °C.

dependent response of the sensor was studied to find the optimum working temperature. Fig. 7a shows the relation between the response of the sensor and operating temperature ranging from 150 °C to 300 °C for pristine ZnO and Ag/ZnO towards hydrogen with a concentration of 300 ppm. The results show that the sensor response increased with an increase in working temperature and reached its maximum value at 250 °C. Further, an increase in working temperature beyond 250 °C decreases the response of the sensor. This behavior is due to the increment in the amount of adsorbed hydrogen with an increase of working temperature, following the improvement of sensing response. This phenomenon is sustained until the temperature reaches the optimum working temperature i.e 250 °C. After that, the response decreased due to the active oxygen species, and tested gas molecules begin to desorb in large quantities. Fig. 7a reveals that the optimum working temperature for both sensors is 250 °C. The dynamic response of ZnO and Ag/ZnO sensor at optimum temperature 250 °C with various concentrations to H_2 gas is presented in Fig. 7b and confirms the behavior of the n-type semiconductor sensor. Generally, the resistance of the n-type semiconductor gas sensor decreases when exposed to reducing gases (H_2), and increases again when exposed to the air atmosphere [39]. Also, Fig. 7b shows the off-state terminal resistance (R_a) that is decreased for the Ag/ZnO sensor compared to the pure ZnO, which suggests lowering band-gap (E_g) due to Ag-doping. The Ag/ZnO sensor also provides stable off-state resistance. In contrast, the bare ZnO sensor shows an increase in off-state resistance which shows the poor stability of the bare ZnO sensor. It may also be due to the slow diffusion of oxygen species into the ZnO crystals and the non-removal of these species out of the lattice. On contrary, due to the spillover effect of Ag catalyst, oxygen molecules are converted into atomic oxygen species, hence make them easy to diffuse into the ZnO lattice, which provides Ag/ZnO sensor steady off-state resistance in a short period [40] it can also be anticipated due to the ease of charge transfer from ZnO-Ag, provide the constant resistance state post 13 endurance cycles also.

The response of pristine ZnO and Ag/ZnO sensors to different H_2 concentrations at temperature 250 °C was shown in Fig. 8. The results show that gas sensing responses for both sensors readily increase with increasing hydrogen concentration from 5 ppm to 300 ppm. It is also demonstrated that the addition of Ag in ZnO enhanced the gas sensing response at each concentration of H_2 in comparison to the pure ZnO sensor. The prepared sensor based on Ag/ZnO microstructures exhibited a maximum response of 479 % in a hydrogen environment, which is 5 times higher than the response of the bare ZnO sensor. The sensing response at a low concentration from 5 ppm to 50 ppm is shown in the inset of Fig. 8 for clear vision and showing the same behavior as observed for high concentration. Moreover, the 4.8 % response was

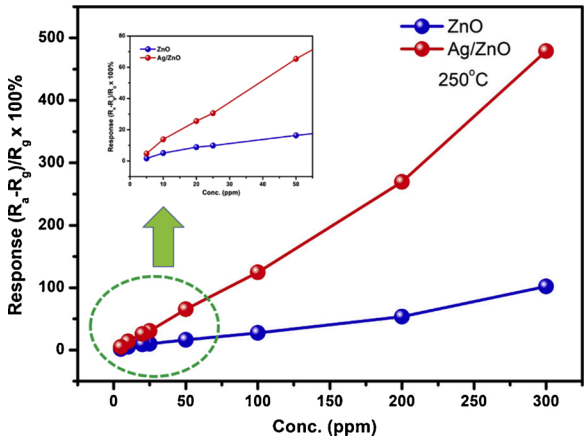

Fig. 8. Gas sensing response of ZnO and Ag/ZnO sensor at different concentrations of hydrogen at 250 °C; inset (enlarge the view of concentration from 5 ppm to 50 ppm).

obtained at 5 ppm H_2 concentration of Ag/ZnO sensor, indicating its utility for detecting the low concentration of hydrogen gas in practical applications.

The response/recovery time, repeatability, and stability are also very important indexes to define sensor performance. Fig. 9a shows the typical response and recovery curve of the bare ZnO and Ag/ZnO sensor under 300 ppm H_2 concentration at 250 °C. The response time T_{res} (reaching 90 % variation in the response upon exposure to gas) and recovery time T_{rec} (sensor to reach 90 % of its initial response) of Ag/ZnO sensor were 175 s and 655 s, respectively, which is shorter than the response time (611 s) and recovery time (1127s) of pure ZnO sensor. Therefore, it is observed that the incorporation of Ag can not only increase the sensing response but also reduces the response and recovery time of pure ZnO. This is because the Ag nanoparticles can increase hydrogen molecules' adsorption and diffusion rate, resulting in a faster response.

Moreover, to check the accuracy of the sensor for real-time monitoring of hydrogen leaks in air, repeatability and stability were measured. To evaluate the repeatability of the Ag/ZnO sensor, the 13 cycles testing towards 300 ppm H_2 at 250 °C was carried out and presented in Fig. 9b. It was observed that the Ag/ZnO sensor presents excellent repeatability with maintained the almost same response within 13 successive sensing tests when switching between hydrogen and air. The average response for 300 ppm hydrogen from these repetitive cycles was found to be 476 % with a relatively minor deviation of 0.48 %. Since Ag/ZnO sensor was the most promising device, long-term stability measurements were performed at 250 °C for 300 ppm hydrogen gas over 30 days and illustrated in Fig. 9c. The stability results demonstrated that good long-term stability is attained over 30 days. Hence, the prepared Ag/ZnO hollow microstructures have great potential for hydrogen detection in practical applications.

The selectivity of the target gas is one of the crucial factors affecting the practical application of the sensor. Therefore, to test the selectivity of the sensor, the response of the pure ZnO and Ag/ZnO to various tested gases, such as carbon monoxide (CO), carbon dioxide (CO_2), and hydrogen (H_2) have been scrutinized with a concentration of 300 ppm at optimal temperature 250 °C and the consequences are shown in Fig. 9d. The selectivity of the sensor is defined as the ratio of its best response to its second-best response [41]. Here, the selectivity was calculated by taking the ratio of response for H_2 to the response for CO or CO_2 gases. The response value of the Ag/ZnO sensor at 250 °C at 300 ppm of H_2, CO, and CO_2 are 479 %, 35 %, and 40 %, respectively. Therefore, the target gas (H_2) selectivity of 300 ppm is about 14 and 12 with respect to CO and CO_2 gases of the same concentration, respectively. That means the detection of H_2 is almost 14 and 12-times more probable from a mixture of equal concentration with CO and CO_2 gases, respectively, which shows an excellent selectivity towards hydrogen of the Ag/ZnO sensor. This is ascribed to the fact that the adsorption energy of H_2 gas is much higher compared to other gases at 250 °C temperature on the sensor surface. Thus, based on the results, it could be revealed that the Ag/ZnO tubes-like hollow microstructures-based sensor demonstrates good repeatability and selectivity towards H_2 and long-term stability which are imperative for its practical application.

The improved hydrogen sensing performance of our Ag/ZnO sensor is compared with other sensors based on ZnO composites, shown in Table 2 and we can state that our sensor has excellent sensitivity with great endurance and have a significant position in the reported work indicating its auspicious applicability for the detection of H_2 gas in real applications.

3.6. Gas sensing mechanism

The gas sensing mechanism depends on the interaction of gas with the gas-sensitive material and the schematic of the gas sensing mechanism is presented in Fig. 10. In chemi-resistive type sensing materials, when a target gas reacts with the material, a change in material

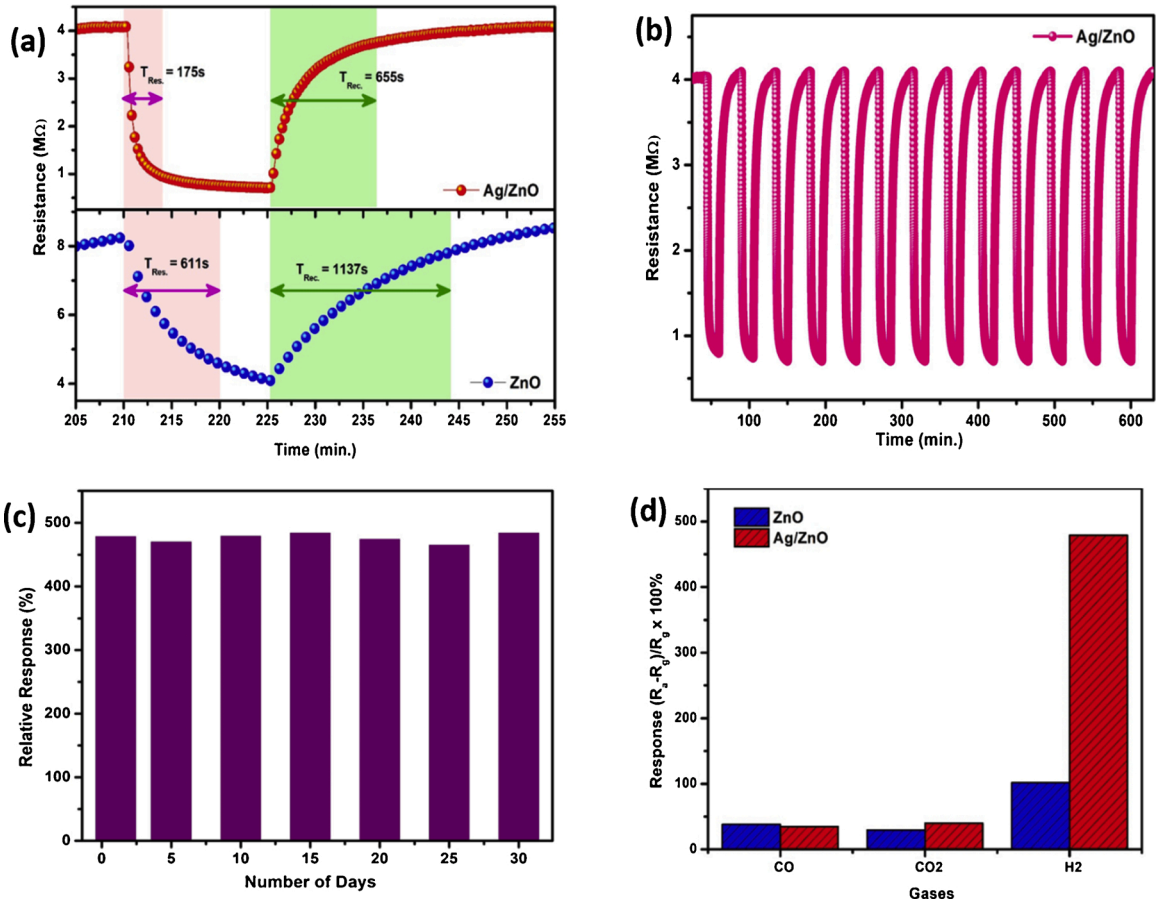

Fig. 9. (a) Comparison of response and recovery time of ZnO and Ag/ZnO sensor to 300 ppm H_2 at 250 °C (b) repeatability testing of Ag/ZnO sensor to 300 ppm H_2 with 13 successive cycles at 250 °C (c) long-term stability over 30 days of Ag/ZnO sensor to 300 ppm H_2 at 250 °C (d) selectivity histogram of ZnO and Ag/ZnO sensor at 250 °C and the Ag/ZnO sensor is highly selective to H_2.

Table 2
A comparison of the gas-sensing performance of reported ZnO nanocomposites to hydrogen.

Method	Sensing material	Working Temp (°C)	H_2 Conc. (ppm)	Sensitivity (S) %	Endurance	Ref.
Chemical bath deposition	ZnO	25	1000	500%[e]	7	[42]
Pulsed laser deposition (PLD)	Pt/Pd bimetallic NPs decorated ZnO nanorods	100	10,000	58%[a]	–	[43]
Chemical vapor deposition	Pd NPs-decorated ZnO nanowires	25	20	3.7%[e]	–	[44]
RF magnetron sputtering	Spherical Au on ZnO thin films	250	1000	172%[c]	6	[31]
Chemical precipitation	Pd/ZnO nanorods	100	10,000	74%[b]	3	[45]
RF magnetron sputtering	Ni doped ZnO nanostructures	150	10,000	69%[a]	–	[11]
RF sputtering	MoS_2/ZnO nanotubes	RT	500	51.1%[d]	20	[46]
Chemical solution deposition	In-doped ZnO thin film	300	5	15%[a]	5	[47]
Chemically co-precipitation	**Ag/ZnO hollow microstructures**	**250**	**300**	479 %[c]	**13**	**This work**

[a] $S = (R_a - R_g)/R_a \times 100$ %.
[b] $S = (R_g - R_a)/R_a \times 100$ %.
[c] $S = (R_a - R_g)/R_g \times 100$ %.
[d] $S = R_g/R_a \times 100$ %.
[e] $S = (I_g - I_a)/I_a \times 100$ %.

resistance is observed [48]. ZnO is an n-type semiconducting metal oxide and electrons are the majority charge carriers. In the presence of air, environmental oxygen interacts with the ZnO surface and diffuses through the grain boundaries, and gets adsorbed at the surface and grain boundaries. This adsorbed oxygen captures electrons from the conduction band of ZnO and makes ionic oxygen species (O_2^-, O^- and O^{2-}) depending on the temperature and the following reactions take place at the interface (Fig. 9a):

$$O_2 \rightarrow O_{2(ads)} \quad (2)$$

$$O_{2(ads)} + e^- \rightarrow O^-_{2(ads)} \quad (3)$$

$$O^-_{2(ads)} + e^- \rightarrow 2O^-_{(ads)} \quad (4)$$

$$O^-_{(ads)} + e^- \rightarrow O^{2-}_{(ads)} \quad (5)$$

As a result, a space charge region is formed at the surface of the material that creates a potential barrier for electron conduction, giving rise to the material's electrical resistance [49]. When a reducing gas like H_2, comes in contact with this material, it reacts with the adsorbed

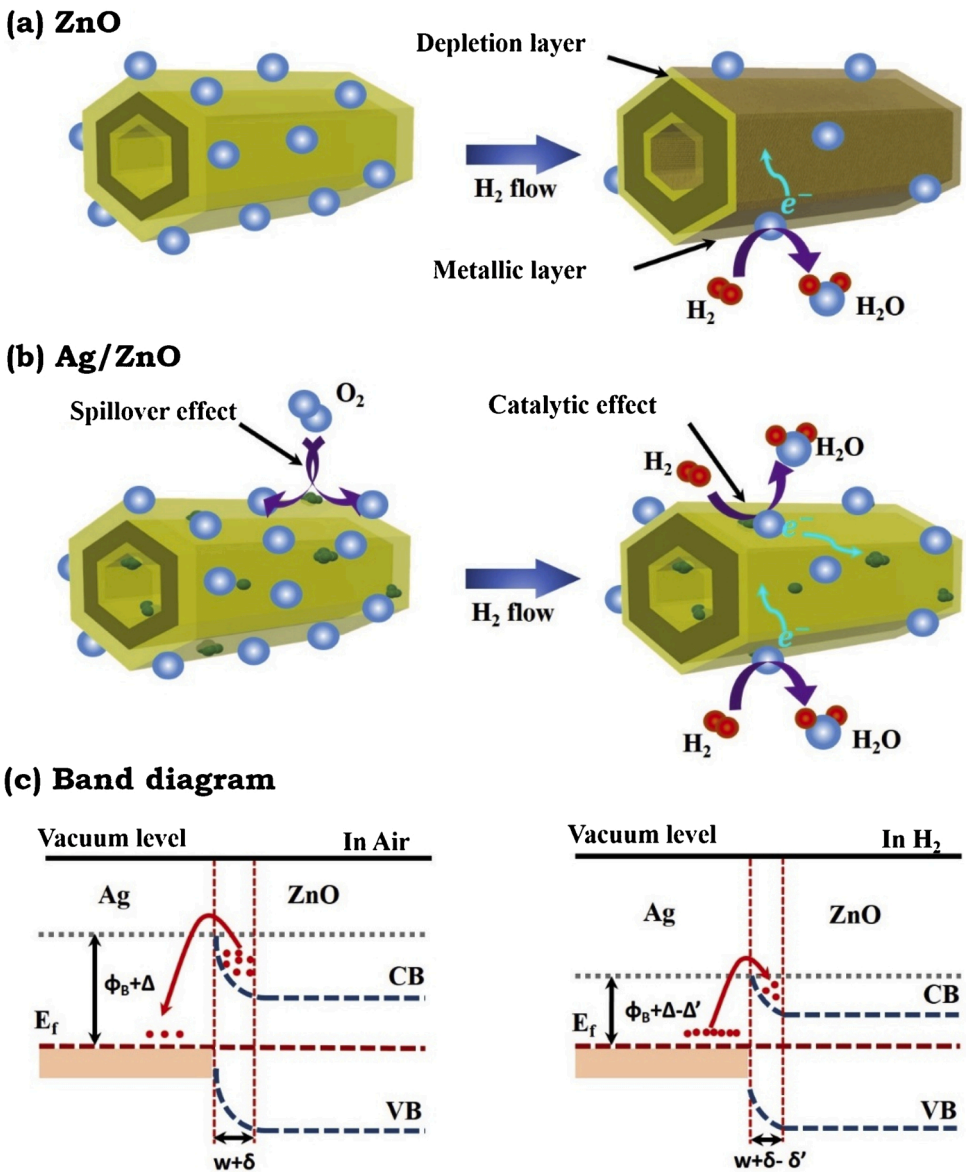

Fig. 10. Schematic for the gas sensing mechanism for (a) ZnO; and (b) Ag/ZnO; (c) band diagram representation for Ag/ZnO in presence of Air and H_2. (where ϕ_B and ware barrier height and depletion layer width at the interface between Ag & ZnO respectively, Δ and Δ' are the change in barrier height in presence of oxygen and H_2 respectively, and δ & δ' are the change in depletion layer width in presence of oxygen and H_2 respectively).

oxygen and the following reaction takes place [50]:

$$H_2 + O^-_{(ads)} \rightarrow H_2O + e^- \quad (6)$$

In turn, these electrons are released back to the conduction band of ZnO, which decreases the height of barrier potential and the depletion layer width, hence the resistance of the material gets decreased [51]. In the case of H_2 gas, surface metallization is also observed at the ZnO surface [52], it is due to the reaction of H_2 molecules with the oxygen present in the crystal, and ZnO is reduced to Zn at the surface. Which also contributes to the decrement in electrical resistance. When target gas is removed from the sensor environment, environmental oxygen again gets adsorbed to the ZnO surface. Since these structures are tube-like structures, gas molecules can interact from outside and inside the tube. In Ag/ZnO microstructures, the response is increasing selectively for H_2 gas. It may be attributed to the chemical sensitization and electronic sensitization in the presence of Ag nanoparticles, shown in Fig. 10b. In chemical sensitization, Ag nanoparticles induce a spill-over effect and increase the number of adsorbed oxygen species and provide the catalytic effect of the reaction occurring between H_2 gas and adsorbed oxygen species. Along with that, due to spill-over effect Ag nanoparticles potentially convert molecular hydrogen into atomic hydrogen and improve the mobility of hydrogen through the grain boundaries, which in turn increase the diffusion rate of hydrogen into the bulk ZnO that leads to enhanced response. On the other hand, electronic sensitization can be expressed in terms of modulation of the charge depletion layer. When Ag nanoparticles are present at the surface of ZnO, depletion layer width is increased near the metal-semiconductor interface. This modulation can be further explained by the band diagram (Fig. 10c).

Many researchers quote that the work function for Ag is about 4.26 eV [53] and for ZnO, it is 4.45 eV [54]. Due to the difference in work function, electrons move towards the Ag from the conduction band of ZnO, and a Schottky barrier is created at the interface of Ag and ZnO as shown in Fig. 10(c), which contributes to the increase in resistance in presence of oxygen [55]. When H_2 gas is introduced to the sensor, the height of this Schottky barrier is decreased as well as the layer width is reduced and electrons are released to the conduction band of ZnO, this decrease improves the response additionally for the Ag/ZnO samples in

comparison to the pure ZnO samples [56]. The selectivity for H_2 may be attributed to the lowest activation energy of H_2 molecules and the smallest size among the other gases which makes it more probable to diffuse into the bulk ZnO nanostructures.

4. Conclusions

In summary, we developed a new hydrogen sensing material based on the ZnO hollow tubes-like microstructures modified with Ag nanoparticles. The Ag/ZnO hybrid was successfully synthesized by using the one-step chemical co-precipitation method and their gas sensing performance was investigated in an operating temperature range of 150–300 °C. It is noteworthy that the addition of Ag nanoparticles in the ZnO sensor improved the gas sensing properties as compared to the pure ZnO sensor. The Ag/ZnO microstructures exhibited a superior response of 479 % with 300 ppm hydrogen at 250 °C. The sensor showed excellent selectivity towards H_2 gas in comparison to CO and CO_2 gas at 300 pm concentration of gas. This increment in the sensing performance could be attributed to Ag nanoparticles' catalytic and spillover effect and the Schottky junctions. Furthermore, the obtained composites exhibit fast response-recovery characteristics, good repeatability, and stability. All these results show that the as-prepared low-cost Ag/ZnO hollow microstructures can be promising materials and make a significant contribution to the application of hydrogen detection.

CRediT authorship contribution statement

Sonalika Agarwal: Methodology, Investigation, Validation, Formal analysis, Writing - original draft, Writing-review & editing. **Sanjay Kumar**: Formal analysis, Investigation, Writing-review & editing. **Himanshu Agrawal:** Analysis, Writing- review & editing. **Mohamad G. Moinuddin:** Investigation, IDEs fabrication. **Manoj Kumar:** Validation, Writing- review & editing. **Satinder K Sharma:** Resources, Writing-review & editing, Funding acquisition. **Kamlendra Awasthi:** Conceptualization, Resources, Writing-review & editing, Supervision, Project administration, Funding acquisition.

Declaration of Competing Interest

The authors report no declarations of interest.

Acknowledgments

The author acknowledges the Department of Science and Technology, Government of India for financial support under the Women Scientist Scheme (reference no. SR/WOS-A/PM-72/2016) and SERB under the ECR project (reference no. ECR/2016/001780). The authors are thankful to MRC, MNIT Jaipur for providing the research facilities.

References

[1] Y. Luo, C. Zhang, B. Zheng, X. Geng, M. Debliquy, Hydrogen sensors based on noble metal doped metal-oxide semiconductor: a review, Int. J. Hydrogen Energy 42 (2017) 20386–20397, https://doi.org/10.1016/j.ijhydene.2017.06.066.

[2] I. Darmadi, F.A.A. Nugroho, C. Langhammer, High-performance nanostructured palladium-based hydrogen sensors - current limitations and strategies for their mitigation, ACS Sens. 5 (2020) 3306–3327, https://doi.org/10.1021/acssensors.0c02019.

[3] P. Singh, S. Bhattacharya, Hydrogen gas sensing methods, materials, and approach to achieve parts per billion level detection: a review, Int. J. Hydrogen Energy 44 (2019) 26076–26099, https://doi.org/10.1016/j.ijhydene.2019.08.052.

[4] A. Katoch, J.H. Kim, Y.J. Kwon, H.W. Kim, S.S. Kim, Bifunctional sensing mechanism of SnO2-ZnO composite nanofibers for drastically enhancing the sensing behavior in H2 gas, ACS Appl. Mater. Interfaces 7 (2015) 11351–11358, https://doi.org/10.1021/acsami.5b01817.

[5] M. Govindhan, B. Sidhureddy, A. Chen, High-temperature hydrogen gas sensor based on three-dimensional hierarchical-nanostructured nickel-cobalt oxide, ACS Appl. Nano Mater. 1 (2018) 6005–6014, https://doi.org/10.1021/acsanm.8b00835.

[6] L. Kumar Jangir, Y. Kumari, A. Kumar, M. Kumar, K. Awasthi, Investigation of luminescence and structural properties of ZnO nanoparticles, synthesized with different precursors, Mater. Chem. Front. 1 (2017) 1413–1421, https://doi.org/10.1039/C7QM00058H.

[7] Y.K. Mishra, R. Adelung, ZnO tetrapod materials for functional applications, Mater. Today 21 (2018) 631–651, https://doi.org/10.1016/j.mattod.2017.11.003.

[8] S. Agarwal, L.K. Jangir, K.S. Rathore, M. Kumar, K. Awasthi, Morphology-dependent structural and optical properties of ZnO nanostructures, Appl. Phys. A. 125 (2019) 553, https://doi.org/10.1007/s00339-019-2852-x.

[9] H. Kim, Y. Pak, Y. Jeong, W. Kim, J. Kim, G.Y. Jung, Amorphous Pd-assisted H2 detection of ZnO nanorod gas sensor with enhanced sensitivity and stability, Sens. Actuators B Chem. 262 (2018) 460–468, https://doi.org/10.1016/j.snb.2018.02.025.

[10] R. Malik, V.K. Tomer, Y.K. Mishra, L. Lin, Functional gas sensing nanomaterials: a panoramic view, Appl. Phys. Rev. 7 (2020), https://doi.org/10.1063/1.5123479.

[11] V.S. Bhati, S. Ranwa, M. Fanetti, M. Valant, M. Kumar, Efficient hydrogen sensor based on Ni-doped ZnO nanostructures by RF sputtering, Sens. Actuators B Chem. 255 (2018) 588–597, https://doi.org/10.1016/j.snb.2017.08.106.

[12] H.J. Le, D. Van Dao, Y.T. Yu, Superfast and efficient hydrogen gas sensor using PdAualloy@ZnO core-shell nanoparticles, J. Mater. Chem. A 8 (2020) 12968–12974, https://doi.org/10.1039/d0ta03552a.

[13] O. Lupan, V. Postica, N. Wolff, J. Su, F. Labat, I. Ciofini, H. Cavers, R. Adelung, O. Polonskyi, F. Faupel, L. Kienle, B. Viana, T. Pauporté, Lowerature solution synthesis of Au-modified ZnO nanowires for highly efficient hydrogen nanosensors, ACS Appl. Mater. Interfaces 11 (2019) 32115–32126, https://doi.org/10.1021/acsami.9b08598.

[14] F. Fan, J. Zhang, J. Li, N. Zhang, R. Hong, X. Deng, Hydrogen sensing properties of Pt-Au bimetallic nanoparticles loaded on ZnO nanorods, Sens. Actuators B. Chem. 241 (2017) 895–903, https://doi.org/10.1016/j.snb.2016.11.025.

[15] Z. Yin, X. Wang, F. Sun, X. Tong, C. Zhu, Q. Lv, D. Ye, S. Wang, W. Luo, Y.A. Huang, Aligned hierarchical Ag/ZnO nano-heterostructure arrays via electrohydrodynamic nanowire template for enhanced gas-sensing properties, Sci. Rep. 7 (2017) 1–10, https://doi.org/10.1038/s41598-017-12553-7.

[16] V. Postica, A. Vahl, D. Santos-Carballal, T. Dankwort, L. Kienle, M. Hoppe, A. Cadi-Essadek, N.H. De Leeuw, M.I. Terasa, R. Adelung, F. Faupel, O. Lupan, Tuning ZnO sensors reactivity toward volatile organic compounds via Ag doping and nanoparticle functionalization, ACS Appl. Mater. Interfaces 11 (2019) 31452–31466, https://doi.org/10.1021/acsami.9b07275.

[17] Z. Shen, X. Zhang, R. Mi, M. Liu, Y. Chen, C. Chen, S. Ruan, On the high response towards TEA of gas sensors based on Ag-loaded 3D porous ZnO microspheres, Sens. Actuators B Chem. 270 (2018) 492–499, https://doi.org/10.1016/j.snb.2018.05.034.

[18] H.R. Yousefi, B. Hashemi, A. Mirzaei, H. Roshan, M.H. Sheikhi, Effect of Ag on the ZnO nanoparticles properties as an ethanol vapor sensor, Mater. Sci. Semicond. Process. 117 (2020), https://doi.org/10.1016/j.mssp.2020.105172, 105172.

[19] Y. Al-Hadeethi, A. Umar, A.A. Ibrahim, S.H. Al-Heniti, R. Kumar, S. Baskoutas, B. M. Raffah, Synthesis, characterization and acetone gas sensing applications of Ag-doped ZnO nanoneedles, Ceram. Int. 43 (2017) 6765–6770, https://doi.org/10.1016/j.ceramint.2017.02.088.

[20] Y. Wei, X. Wang, G. Yi, L. Zhou, J. Cao, G. Sun, Z. Chen, H. Bala, Z. Zhang, Hydrothermal synthesis of Ag modified ZnO nanorods and their enhanced ethanol-sensing properties, Mater. Sci. Semicond. Process. 75 (2018) 327–333, https://doi.org/10.1016/j.mssp.2017.11.007.

[21] S.G. R, M. Navaneethan, V.L. Patil, S. Ponnusamy, C. Muthamizhchelvan, S. Kawasaki, P.S. Patil, Y. Hayakawa, Sensitivity enhancement of ammonia gas sensor based on Ag/ZnO flower and nanoellipsoids at low temperature, Sens. Actuators B Chem. 255 (2018) 672–683, https://doi.org/10.1016/j.snb.2017.08.015.

[22] S. Wang, F. Jia, X. Wang, L. Hu, Y. Sun, G. Yin, T. Zhou, Z. Feng, P. Kumar, B. Liu, Fabrication of ZnO nanoparticles modified by uniformly dispersed Ag nanoparticles: enhancement of gas sensing performance, ACS Omega 5 (2020) 5209–5218, https://doi.org/10.1021/acsomega.9b04243.

[23] Q. Zhang, Z. Pang, W. Hu, J. Li, Y. Liu, Y. Liu, F. Yu, C. Zhang, M. Xu, Performance degradation mechanism of the light-activated room temperature NO2 gas sensor based on Ag-ZnO nanoparticles, Appl. Surf. Sci. 541 (2021), https://doi.org/10.1016/j.apsusc.2020.148418, 148418.

[24] J. Ding, J. Zhu, P. Yao, J. Li, H. Bi, X. Wang, Synthesis of ZnO-Ag hybrids and their gas-sensing performance toward ethanol, Ind. Eng. Chem. Res. 54 (2015) 8947–8953, https://doi.org/10.1021/acs.iecr.5b01711.

[25] T. Dilova, G. Atanasova, A.O. Dikovska, N.N. Nedyalkov, The effect of light irradiation on the gas-sensing properties of nanocomposites based on ZnO and Ag nanoparticles, Appl. Surf. Sci. 505 (2020), https://doi.org/10.1016/j.apsusc.2019.144625, 144625.

[26] L. Zhou, J. Bai, Y. Liu, F. Liu, H. Wang, Y. Zhang, G. Lu, Highly sensitive C2H2 gas sensor based on Ag modified ZnO nanorods, Ceram. Int. 46 (2020) 15764–15771, https://doi.org/10.1016/j.ceramint.2020.03.120.

[27] Y.T. Tsai, S.J. Chang, L.W. Ji, Y.J. Hsiao, I.T. Tang, H.Y. Lu, Y.L. Chu, High sensitivity of NO gas sensors based on novel Ag-doped ZnO nanoflowers enhanced with a UV light-emitting diode, ACS Omega 3 (2018) 13798–13807, https://doi.org/10.1021/acsomega.8b01882.

[28] S. Verhaverbeke, J.W. Parker, C.F. McConnell, The role of HO2 − in SC-1 cleaning solutions, MRS Proc. 477 (1997) 47, https://doi.org/10.1557/PROC-477-47.

[29] H.S, S.K.S.S. Sharma, S. Das, R. Khosla, Realization and performance analysis of facile-processed μ -IDE-based multilayer HfS2/HfO2 transistors, IEEE Trans. Electron Devices 66 (2019) 3236–3241.

[30] I. Kortidis, H.C. Swart, S.S. Ray, D.E. Motaung, Characteristics of point defects on the room temperature ferromagnetic and highly NO2 selectivity gas sensing of p-type Mn3O4 nanorods, Sens. Actuators B Chem. 285 (2019) 92–107, https://doi.org/10.1016/j.snb.2019.01.007.
[31] G.S. Kumar, L. Xuejin, Y. Du, Y. Geng, X. Hong, UV-light enhanced high sensitive hydrogen (H2) sensor based on spherical Au nanoparticles on ZnO nano-structured thin films, J. Alloys Compd. 798 (2019) 467–477, https://doi.org/10.1016/j.jallcom.2019.05.227.
[32] B. Liu, H.C. Zeng, Direct growth of enclosed ZnO nanotubes, Nano Res. 2 (2009) 201–209, https://doi.org/10.1007/s12274-009-9018-7.
[33] H.H. Mai, D.H. Tran, E. Janssens, Non-enzymatic fluorescent glucose sensor using vertically aligned ZnO nanotubes grown by a one-step, seedless hydrothermal method, Microchim. Acta. 186 (2019) 2–11, https://doi.org/10.1007/s00604-019-3353-5.
[34] T. Chitradevi, A. Jestin Lenus, N. Victor Jaya, Structure, morphology and luminescence properties of sol-gel method synthesized pure and Ag-doped ZnO nanoparticles, Mater. Res. Express 7 (2019), https://doi.org/10.1088/2053-1591/ab5c53.
[35] S. Kumar, V. Singh, A. Tanwar, Structural, morphological, optical and photocatalytic properties of Ag-doped ZnO nanoparticles, J. Mater. Sci. Mater. Electron. 27 (2016) 2166–2173, https://doi.org/10.1007/s10854-015-4227-1.
[36] S.M. Hosseini, I.A. Sarsari, P. Kameli, H. Salamati, Effect of Ag doping on structural, optical, and photocatalytic properties of ZnO nanoparticles, J. Alloys Compd. 640 (2015) 408–415, https://doi.org/10.1016/j.jallcom.2015.03.136.
[37] Y. Liang, N. Guo, L. Li, R. Li, G. Ji, S. Gan, Fabrication of porous 3D flower-like Ag/ZnO heterostructure composites with enhanced photocatalytic performance, Appl. Surf. Sci. 332 (2015) 32–39, https://doi.org/10.1016/j.apsusc.2015.01.116.
[38] Y.T. Tsai, S.J. Chang, L.W. Ji, Y.J. Hsiao, I.T. Tang, H.Y. Lu, Y.L. Chu, High sensitivity of NO gas sensors based on novel Ag-Doped ZnO nanoflowers enhanced with a UV light-emitting diode, ACS Omega 3 (2018) 13798–13807, https://doi.org/10.1021/acsomega.8b01882.
[39] S. Agarwal, P. Rai, E. Navarrete, E. Llobet, F. Güell, M. Kumar, K. Awasthi, Gas sensing properties of ZnO nanostructures (flowers/rods) synthesized by hydrothermal method, Sens. Actuators B. Chem. 292 (2019) 24–31, https://doi.org/10.1016/j.snb.2019.04.083.
[40] Z.S. Hosseini, A. Mortezaali, A. Iraji Zad, S. Fardindoost, Sensitive and selective room temperature H2S gas sensor based on Au sensitized vertical ZnO nanorods with flower-like structures, J. Alloys Compd. 628 (2015) 222–229, https://doi.org/10.1016/j.jallcom.2014.12.163.
[41] M. Tonezzer, S.C. Izidoro, J.P.A. Moraes, L.T.T. Dang, Improved gas selectivity based on carbon modified SnO2 nanowires, Front. Mater. 6 (2019) 1–9, https://doi.org/10.3389/fmats.2019.00277.
[42] J.J. Hassan, M.A. Mahdi, C.W. Chin, H. Abu-Hassan, Z. Hassan, A high-sensitivity room-temperature hydrogen gas sensor based on oblique and vertical ZnO nanorod arrays, Sens. Actuators B Chem. 176 (2013) 360–367, https://doi.org/10.1016/j.snb.2012.09.081.
[43] K. Hassan, G.S. Chung, Catalytically activated quantum-size Pt/Pd bimetallic core–shell nanoparticles decorated on ZnO nanorod clusters for accelerated hydrogen gas detection, Sens. Actuators B Chem. 239 (2017) 824–833, https://doi.org/10.1016/j.snb.2016.08.084.
[44] S. Ren, G. Fan, S. Qu, Q. Wang, Enhanced H2 sensitivity at room temperature of ZnO nanowires functionalized by Pd nanoparticles, J. Appl. Phys. 110 (2011), https://doi.org/10.1063/1.3647310.
[45] M.F. Bin Alam, D.T. Phan, G.S. Chung, Palladium nanocubes decorated on a one-dimensional ZnO nanorods array for use as a hydrogen gas sensor, Mater. Lett. 156 (2015) 113–117, https://doi.org/10.1016/j.matlet.2015.05.007.
[46] A. Kothandan, B. Huang, D. Kathiravan, A. Saravanan, A. Prasannan, H. Tsai, S. Chen, Effect of MoS 2 solution on reducing the wall thickness of ZnO nanotubes to enhance their hydrogen gas sensing properties, J. Alloys Compd. 854 (2021), https://doi.org/10.1016/j.jallcom.2020.157102, 157102.
[47] S. Pati, P. Banerji, S.B. Majumder, Properties of indium doped nanocrystalline ZnO thin films and their enhanced gas sensing performance, RSC Adv. 5 (2015) 61230–61238, https://doi.org/10.1039/c5ra10919a.
[48] C. Peng, J. Guo, W. Yang, C. Shi, M. Liu, Y. Zheng, J. Xu, P. Chen, T. Huang, Y. Yang, Synthesis of three-dimensional flower-like hierarchical ZnO nanostructure and its enhanced acetone gas sensing properties, J. Alloys Compd. 654 (2016) 371–378, https://doi.org/10.1016/j.jallcom.2015.09.120.
[49] L. Wang, Y. Kang, X. Liu, S. Zhang, W. Huang, S. Wang, ZnO nanorod gas sensor for ethanol detection, Sens. Actuators B Chem. 162 (2012) 237–243, https://doi.org/10.1016/j.snb.2011.12.073.
[50] O. Lupan, V.V. Ursaki, G. Chai, L. Chow, G.A. Emelchenko, I.M. Tiginyanu, A. N. Gruzintsev, A.N. Redkin, Selective hydrogen gas nanosensor using individual ZnO nanowire with fast response at room temperature, Sens. Actuators B Chem. 144 (2010) 56–66, https://doi.org/10.1016/j.snb.2009.10.038.
[51] S. Agarwal, S. Kumar, E. Navarrete, M. Kumar, E. Llobet, K. Awasthi, Materials Letters: X Facile synthesis of Pd @ ZnO core @ shell nanoparticles for selective ethanol detection, Mater. Lett. X 10 (2021) 100068, https://doi.org/10.1016/j.mlblux.2021.100068.
[52] A. Katoch, S.W. Choi, H.W. Kim, S.S. Kim, Highly sensitive and selective H2 sensing by ZnO nanofibers and the underlying sensing mechanism, J. Hazard. Mater. 286 (2015) 229–235, https://doi.org/10.1016/j.jhazmat.2014.12.007.
[53] S. Ghosh, V.S. Goudar, K.G. Padmalekha, S.V. Bhat, S.S. Indi, H.N. Vasan, ZnO/Ag nanohybrid: synthesis, characterization, synergistic antibacterial activity and its mechanism, RSC Adv. 2 (2012) 930–940, https://doi.org/10.1039/c1ra00815c.
[54] A.F. Abdulrahman, S.M. Ahmed, A.A. Barzinjy, S.M. Hamad, N.M. Ahmed, M. A. Almessiere, Fabrication and characterization of high-quality UV photodetectors based ZnO nanorods using traditional and modified chemical bath deposition methods, Nanomaterials 11 (2021) 1–26, https://doi.org/10.3390/nano11030677.
[55] A.N. Kadam, D.P. Bhopate, V.V. Kondalkar, S.M. Majhi, C.D. Bathula, A.V. Tran, S. W. Lee, Facile synthesis of Ag-ZnO core–shell nanostructures with enhanced photocatalytic activity, J. Ind. Eng. Chem. 61 (2018) 78–86, https://doi.org/10.1016/j.jiec.2017.12.003.
[56] D.K. Kwon, Y. Porte, K.Y. Ko, H. Kim, J.M. Myoung, High-performance flexible ZnO nanorod UV/gas dual sensors using Ag nanoparticle templates, ACS Appl. Mater. Interfaces 10 (2018) 31505–31514, https://doi.org/10.1021/acsami.8b13046.

Sonalika Agarwal is working as Women Scientist (DST) in Department of Physics, MNIT Jaipur, India. She received her Ph. D degree in the area of polymer nanocomposites from University of Rajasthan, Jaipur, India on 2012. She has worked as Assistant Professor at KIET group of institutions, Ghaziabad. Currently her research interests include the synthesis of different nanostructures of metal oxides and their applications in gas sensors.

Sanjay Kumar received his master's degree in 2017 from PDU Shekhawati University, Sikar, Rajasthan and now he is pursuing Ph.D. from the Department of Physics, MNIT Jaipur, India. His work is based on Encapsulated and Functionalized Metal Oxide Nanostructures for Gas Sensing Applications.

Himanshu Agrawal received his master's degree in from PDU Shekhawati University, Sikar, Rajasthan and University of Rajasthan, Jaipur. He is working on flexible gas sensors for his PhD degree from the Department of Physics, MNIT Jaipur, India.

Mohamad Ghulam Moinuddin: received B.Sc in Applied Physics from University of Delhi in 2013 and M.Sc. in Electronic Science from the Jamia Millia Islamia, New Delhi, in 2015. Currently, he is pursuing Ph.D. degree in VLSI from Indian Institute of Technology Mandi, India. His research interest includes nano-electronics/spintronics devices and nano-lithography application.

Manoj Kumar is an Assistant Professor in Department of Physics, Malaviya National Institute of Technology Jaipur, India. He completed his Ph.D. in Physics from University of Rajasthan, Jaipur on 2010. He has worked in Max Planck Institute for Chemical Physics of Solids and in Institute of Solid State Physics, IFW Dresden, Germany as a post-doctoral fellow. His core area of research includes nanocomposites, nanomaterials, CNTs and their devices, thermoelectric power generators, topological insulators and 2DEG materials at high pressures (0–200 kbar), low temperatures (300 m K-300 K) and high magnetic fields (0−17 T), synthesis and characterization of nano-crystalline, thin films and bulk single crystals through different routes.

Satinder K. Sharma received the Ph.D. degree from the Department of Electronic Science, Kurukshetra University, Kurukshetra, India, in 2007. From 2007 to 2010, he was a Post-Doctoral Fellow with the DST Unit on Nanosciences, Department of Chemical Engineering (CHE), IIT Kanpur, Kanpur, India and from 2010 to 2012, at Indian Institute of Information Technology, Allahabad, India as an Assistant Professor. From 2012, he is working at School of Computing and Electrical Engineering, IIT Mandi, Himachal Pradesh, India. He has authored or coauthored more than 75 publications in the international peer-reviewed journals. His current research interests include micro/nanoelectronics, CMOS device fabrication and characterization, MEMS and NEMS, nanocomposite, sensors, photovoltaic, and self-assembly.

Kamlendra Awasthi earned his Ph.D. degree from the University of Rajasthan, Jaipur India in 2007. Dr. Awasthi is an Assistant Professor in the Department of Physics and is currently working as Head, Materials Research Centre at Malaviya National Institute of Technology Jaipur, India. He has worked at Nanoscience Center, Indian Institute of Technology Kanpur, India as Research Scientist, and at Leibniz Institute of Polymer Research Dresden Germany as an Alexander von Humboldt Fellow prior to joining Malaviya National Institute of Technology Jaipur in 2012. His main research area is soft materials with a major focus on polymer nanofillers and nanostructured materials for photovoltaic, sensor, and nanofabrication applications. He has authored/co-authored more than 90 publications and edited the special issues in various journals. He is the organizer of a series of International Conferences on Soft Materials held every two years from 2014 onwards. Dr. Awasthi is the recipient of reputed fellowships: Young Scientist (2008) Department of Science and Technology, Govt. of India; Alexander von Humboldt fellowship (2009) by Humboldt foundation Germany; INSPIRE faculty award (2012) from the Department of Science and Technology, Govt. of India and Early Career Research Award (2017) from SERB-New Delhi, India.